Contents lists available at ScienceDirect

Computational Materials Science

journal homepage: http://ees.elsevier.com

Prenucleation at the liquid-Al/α-Al_2O_3 and the liquid-Al/MgO interfaces

Changming Fang*, Zhongyun Fan

BCAST, Brunel University London, Uxbridge, Middlesex UB8 3PH, United Kingdom

ARTICLE INFO

Keywords
Prenucleation
Liquid-metal/oxide interfaces
Ab initio molecular dynamics simulations
Epitaxial nucleation

ABSTRACT

Prenucleation refers to the atomic ordering in the liquid adjacent to a liquid/substrate interface above the nucleation temperature. It provides a precursor for heterogeneous nucleation in the liquid adjacent to the interface. As magnesia (MgO) and alumina (Al_2O_3) widely exist in and can be potential nucleation sites for Al-Mg based alloys, we investigate the influences of the substrate surfaces, the α-Al_2O_3{0 0 0 1} and the Al-terminated MgO{1 1 1} on the atomic ordering in the liquid Al adjacent to the liquid-Al/oxide interfaces using an *ab initio* molecular dynamics simulation technique. The study reveals the formation of an Al-layer terminating the substrates. The newly formed Al-layers display structural splitting and possess atomic vacancies, being atomically rough. Consequently, there is weak prenucleation at the liquid/oxide interfaces. Analysis also exposes subtle influences of the structural and chemical properties of the oxide substrates on the prenucleation at the interfaces. The attained information sheds light on the role of oxide particles in the solidification of Al-Mg based alloys.

1. Introduction

The classical nucleation theory (CNT) suggests that in heterogeneous nucleation a solid substrate can reduce the energy barrier to nucleate a solid phase [1–3]. Consequently, heterogeneous nucleation happens in most solidification processes, whereas homogeneous nucleation hardly occurs [1,4]. The epitaxial nucleation model [4] proposes that heterogeneous nucleation occurs in a layer-by-layer mechanism. The atomic arrangement of the substrate surface supplies a structural template for heterogeneous nucleation. The atomic ordering in the liquid adjacent to the liquid/substrate interface therefore, plays a crucial role in the heterogeneous nucleation processes [4–6]. We define this atomic ordering in the liquid adjacent to the liquid/substrate interface above the nucleation temperature as prenucleation [6,7]. It provides a precursor for heterogeneous nucleation of alloys.

Oxides, such as magnesia (MgO) and alumina (Al_2O_3), form during melting and liquid metal handling in the casting processes [8–15]. The oxide particles have nontrivial influences on the chemical and mechanical properties of the solidified alloys. Experiments revealed that oxide particles, including MgO and Al_2O_3, are potential nucleation sites in Al-Mg based alloys [10–15]. Moreover, oxide particles were observed to be potential nucleation sites for intermetallic compounds [16]. Therefore, knowledge about the prenucleation at the liquid metal/oxide interfaces is important to understand the heterogeneous nucleation processes during the solidification of Al-Mg based alloys.

The ground-state phase of alumina is α-Al_2O_3 with the mineral name corundum. Its lattice can be described in a hexagonal cell [17]. Along the [0 0 0 1] orientation of the hexagonal cell, the crystal structure consists of alternatively an O- and an Al-layer, as shown in Fig. 1a. The oxygen layer has a two dimensional (2D) close-packed hexagonal lattice. Two thirds of the octahedral sites between neighboring O layers are occupied by Al. The Al-layer is uneven and consists of 2-Al sublayers, the Al1 and the Al2 as labelled in Fig. 1a. Consequently, each Al in α-Al_2O_3 is in a distorted octahedron of O, whereas each O is in a distorted tetragon of Al (Fig. 1b).

MgO has the mineral name periclase and exhibits the salt-rock type structure with a face-centred cubic (FCC) lattice [18]. Along its [1 1 1] orientation the structure is composed of alternatively an O- and an Mg-layer (Fig. 1d). The O and the Mg layers have a 2D hexagonal lattice. The sites between neighboring O layers are fully occupied. Both Mg and O atoms are in octahedral coordination, as shown in Fig. 1c.

In common, both α-Al_2O_3{0 0 0 1} and MgO{1 1 1} contain O-layers which exhibit 2D close-packed hexagonal lattices. The major structural differences of the two oxides are the occupation ratios of the terminating sites, the smoothness of the metal layers and the coordination of O by the metals. These differences should affect the prenucleation at the liquid-Al/oxide interfaces.

Chemically, both Al_2O_3 and MgO are ionic compounds corresponding to the large differences in the electronegativity values between the metals (1.61 for Al, 1.31 for Mg, in Pauling scale) and O (3.44). The structure and properties of a crystal is determined by the interaction of the valence electrons of the elements in the crystal. Electronic structure

* Corresponding author.
E-mail address: Changming.Fang@brunel.ac.uk (C. Fang)

https://doi.org/10.1016/j.commatsci.2019.109258
Received 15 July 2019; Received in revised form 27 August 2019; Accepted 29 August 2019
Available online xxx
0927-0256/

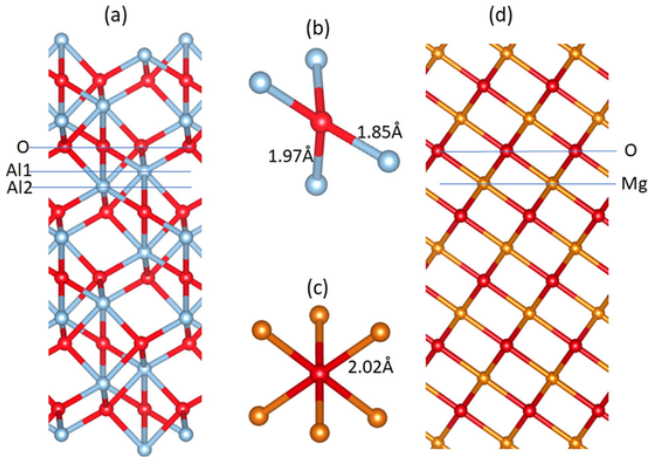

Fig. 1. Schematic structures of α-Al_2O_3 along the [0 0 0 1] orientation (a) and of MgO along its [1 1 1] orientation (d), respectively. Fig. 1b and c display the coordination of O in α-Al_2O_3 and MgO, respectively. The silvery spheres represent Al, the golden Mg and the red O. The labels Al1, Al2 in (1a), Mg (1b), and O (1a and 1b) represent the Al sublayers, the Mg and O layer in the structure, respectively. The Al-O and Mg-O bond-lengths are shown in 1b and 1c, respectively. (For interpretation of the references to color in this figure legend, the reader is referred to the web version of this article.)

theory provided that both the valence bands and lower parts of the conduction bands of MgO and α-Al_2O_3 are dominated by the O 2p and O 3s states, respectively, which suggests that the structures of these ionic oxides are determined mainly by the O sub-lattices [19,20]. Therefore, it is rational to consider the dense O-layer in both oxides as the termination layer. These surfaces of the ionic crystals, e.g. the O-terminated α-Al_2O_3{0 0 0 1} and MgO{1 1 1} substrates contain net charges, being polar and are therefore, unstable at ambient conditions [21,22]. However, this issue can be different when a polar surface is in a condensed metallic condition, whereby the free electrons of metals can compensate the net charges at the substrate surface [23].

Both experimental and theoretical efforts have been committed to obtain information about the atomic ordering in the liquid adjacent to the metal/oxide interfaces [8–15,24–35]. Early works focused on absorption of metallic metals including aluminium on MgO and α-Al_2O_3 surfaces [28,36], on wetting and de-wetting of aluminium on the oxide surface [29,30] and on the orientation relationship of Al/α-Al_2O_3 [33–35]. Using the high resolution transmission electron microscopy (HR-TEM), Medlin *et al* observed a sharp interface with the orientation relationship, α-Al{1 1 1}/α-Al_2O_3{0 0 0 1} [34]. Recently, experiments were performed to investigate layering in the liquid adjacent to the interfaces between liquid Al and α-Al_2O_3{0 0 0 1} using different techniques [24–27]. Using X-ray scattering method, Oh and co-workers observed pronounced layering in the liquid Al adjacent to the α-Al_2O_3{0 0 0 1} substrate [24]. Ma, et al. employed the X-ray crystal truncation rod approach and found only two Al-layers in the liquid adjacent to the L-Al/α-Al_2O_3{0 0 0 1} interface [27]. Overall, experimental observations provided different content of layering in the liquid at the interface [24–27]. This is due to the different techniques, the experimental conditions and the experimental difficulties that liquid aluminium is chemically active to e.g. oxygen, carbon oxides, and water molecules, which always exist in reaction chambers. In this aspect, theoretical approaches can be helpful. Semiempirical atomistic molecular dynamics simulations were utilized to investigate the atomic ordering at solid/liquid interfaces [5,6,37], the influence of lattice misfits of substrates on the atomic ordering in the liquid adjacent to the interfaces [5,6], as well as the impact of atomically rough substrate surfaces on the atomic ordering in the liquid [38]. Parameter-free *ab initio* molecular dynamics (*AI*MD) technique was applied to investigate the effect of substrate chemistry on the prenucleation at the liquid/solid interfaces [7]. The *AI*MD technique was also used to investigate the prenucleation at the L-Al/α-Al_2O_3{0 0 0 1} interfaces [24,27], and at the L-Mg/MgO interfaces [23].

In this paper, we investigate the prenucleation at the liquid-Al/α-Al_2O_3{0 0 0 1} and liquid-Al/MgO{1 1 1} interfaces in a comparative way. The simulations unveil subtle influence of the substrate structures and chemical nature on the prenucleation at the two interfaces. This study provides insight into the heterogeneous nucleation of Al-Mg based alloys.

2. Methods

2.1. Supercells for AIMD simulations

All *ab initio* molecular dynamics simulations were performed at temperature above the liquidus of Al. Thermal expansions of Al and the oxides were therefore, taken into account [17,18,39]. We built systems with different substrate surfaces (Table 1). For the L-Al/α-Al_2O_3{0 0 0 1} systems, the built supercells are hexagonal with the in-plane parameter, $a \approx 3a_o = 14.40$ Å (a_o is the in-plane lattice parameter of α-Al_2O_3 at the simulation temperature [17]). The labels 1Al and 2Al represent the number of Al sublayers (Fig. 1a and the Remarks in Table 1) in the terminating Al-layer. Table 1 also includes the configurations for the L-Al/MgO{1 1 1}$_O$ system, which has a hexagonal supercell with $a \approx 3.615a_o = 14.91$ Å (a_o is the lattice parameter of the fcc MgO [18]) and $c = 48.50$ Å. This supercell contains 450 Al in the liquid and 100O and 75 Mg in the substrate (Table 1). This variety of supercell sizes and the substrate terminations is useful to attain statistically meaningful results, and to avoid possible results from a single starting configuration [40,41]. The large supercells are required for avoiding risk of artificial crystallization of the liquid Al.

2.2. Computational settings

We utilize the first-principles code VASP (Vienna *Ab initio* Simulation Package). It is based on a pseudo-potential plane-wave approach within the density-functional theory (DFT) [42,43]. VASP employs the projector augmented-wave (PAW) method [44,45]. Moreover, it allows variable fractional occupation numbers and therefore, works well for the insulating/metallic systems [42]. This *AI*MD simulation technique uses the finite-temperature density functional theory of the one-electron states, and the Nosé dynamics for generating a canonical NVT ensemble [42]. The used exchange and correlation terms are described within the generalized gradient approximation (GGA-PBE) [46]. The atomic electronic configurations in the pseudo-potentials are Mg ([Ne] $3s^23p^0$), Al ([Ne] $3s^23p^1$) and O ([He] $2s^22p^4$). We utilized the cut-off

Table 1
The L-Al/oxide interfaces built for the *AI*MD simulations. All the lattices are hexagonal. The subscript 1Al means only 1-Al (Al1 in Fig. 1) sublayer and 2Al sublayers (Al1 and Al2) terminating the α-Al_2O_3{0 0 0 1} substrate.

Systems	Lattice parameters(Å)	Numbers of atoms	Remarks on substrate
L-Al/α-Al_2O_3{0 0 0 1}$_{1Al}$	$a = 14.40$, $c = 55.31$	Substrate: 81O, 54 Al Liquid Al: 504	1-Al (Al1) sublayer termination
L-Al/α-Al_2O_3{0 0 0 1}$_{2Al}$	$a = 14.40$, $c = 53.57$	Substrate: 81O, 73 Liquid Al: 468	2-Al (Al1 + Al2) sublayers termination
L-Al/α-Al_2O_3{0 0 0 1}$_O$	$a = 14.40$, $c = 51.82$	Substrate: 81O, 36 Al Liquid Al: 486	O-termination
L-Al/α-Al_2O_3{0 0 0 1}$_{2Al}$	$a = 14.40$, $c = 40.21$	Substrate: 108O, 90 Al Liquid Al: 270	2-Al sublayers termination
L-Al/MgO{1 1 1}$_O$	$a = 14.91$, $c = 48.50$	Substrate: 100O, 75 Mg Liquid Al: 425	O-termination

energies for the wave functions (400.0 eV) and for the augmentation functions (600.0 eV) for structural optimizations, respectively. The electronic wave functions were sampled on dense grids, e.g. a 24 × 24 × 24 (365 *k*-points) and 16 × 16 × 8 *k*-mesh (183 ***k***-points) in the irreducible Brillouin zone (BZ) of the conventional cubic cell of MgO and the hexagonal cell of α-Al_2O_3, respectively using the Monkhorst-Pack approach [47]. For the MD simulations of the large supercells, we employed a cut-of energy of 320 eV and only the Γ-point in the BZs. Our test simulations using the cut-off energies ranging from 200.0 eV to 400.0 eV demonstrated validity of the settings.

Liquid Al was first produced by equilibrating at 3000 K for 2000 steps (1.5 fs (femtoseconds) per step). Then the produced liquid Al samples were cooled to the designed temperature (1000 K). The obtained liquid Al samples and the substrates were used to build the interfaces, which are shown in Table 1. We used two approaches in simulations of the systems. One is to relax all the atoms/ions at beginning. Another way contains two steps: first step is simulating the interfaces with the O atoms in the substrates being fixed for 1000 steps or 1.5 ps (picoseconds). The second step is to simulate the systems by full relaxation of all atoms for another 4000–7000 steps. These simulations provide statistically meaning results. We also performed simulations for selected systems with the pinned O method for sake of comparison. We employed the time-averaged method for sampling the interfaces over a period of time, typically 3.0 ps to 4.5 ps to provide statistically meaningful results [40,48].

2.3. Atomic density profile and in-plane ordering parameter

To provide a quantitative description of the prenucleation at the liquid/solid interfaces we employed two parameters [5–7,12,37]. One is the atomic density profile:

$$\rho(z) = \langle N_z(t) \rangle / \left(L_x L_y \Delta z\right) \quad (1)$$

where, L_x and L_y are the in-plane x and y dimensions, respectively. z is the third perpendicular to the interface. Δz is the bin width (= 0.2 Å in this study) and $N_z(t)$ is the number of atoms between $z - (\Delta z/2)$ and $z + (\Delta z/2)$ at time t. $\langle N_z(t) \rangle$ represents the time-averaged number of atoms of the simulation duration. The profile quantifies the layering in the liquid adjacent to the interfaces.

Another one is the in-plane order parameter, $S(z)$:

$$S(z) = \left[\sum \exp\left(iQ \cdot r_j\right)\right]^2 / N_z^2 \quad (2)$$

where, the summation is over all atoms within a given bin of width, $\Delta z = z - (\Delta z/2)$ and $z + (\Delta z/2)$. $\boldsymbol{Q}$ is the reciprocal lattice vector, $\boldsymbol{r}_j$ is the Cartesian coordinates of the jth atom, and N_z is the number of atoms in the layer. $S(z)$ assesses the atomic ordering in an individual layer.

3. Simulation results

We here present the results of first-principles structural optimizations for the elemental solid and related oxides. The calculations produced the lattice parameters, a = 4.039 Å for the FCC α-Al (experimental value: a = 4.049 Å [39]), and a = 4.195 Å for the FCC MgO (experimental value: a = 4.211 Å [18]). The calculated lattice parameters are: a = 4.807 Å, c = 13.116 Å for the hexagonal α-Al_2O_3, which are close to experimental data: a = 4.758 Å, c = 12.996 Å [17]. Clearly, the calculations reproduced the experimental data. This justifies our approach and the settings.

3.1. Evolutions of the interfaces with different starting configurations

We first analyse the atomic evolutions of the liquid Al adjacent to the interfaces with different starting configurations during the *ab initio* MD simulations. Here we present the atomic evolutions of liquid Al on three substrates: The O-terminated α-Al_2O_3{0 0 0 1} (L-Al/α-Al_2O_3{0 0 0 1}$_O$); The α-Al_2O_3{0 0 0 1} substrate terminated by 1-Al sublayer (L-Al/α-Al_2O_3{0 0 0 1}$_{1Al}$) and the α-Al_2O_3{0 0 0 1} substrate terminated by 2-Al sublayers (L-Al/α-Al_2O_3{0 0 0 1}$_{2Al}$) (Table 1). Selected snapshots of the atomic evolutions during the simulations are displayed in Fig. 2. To obtain some impression about the thermal equilibrating processes, we plotted the dependence of the total valence-electron energy of the L-Al/α-Al_2O_3{0 0 0 1}$_{2Al}$ system during the *AI*MD dynamics simulations at 1000 K in Fig. 3 as an example.

The study produces two types of atomic evolutions at the interfaces: i) On the α-Al_2O_3{0 0 0 1}$_O$ substrate (Fig. 2a), the liquid Al atoms adjacent to the substrate move quickly to the O layer, forming a new Al terminating layer. Similar behavior occurs for the liquid Al atoms adjacent to the L-Al/MgO{1 1 1}$_O$ interface (not shown here); ii) On the α-Al_2O_3{0 0 0 1}$_{1Al}$ substrate (Fig. 2b), the liquid Al atoms adjacent to the interfaces move to the substrates. The Al atoms from the liquid become mixed with the original Al atoms near the O atoms, forming a new Al-terminating layer. As shown in Fig. 2c, the atoms evolution of the liquid Al atoms at the L-Al/α-Al_2O_3{0 0 0 1}$_{2Al}$ interface is similar to the latter type. Fig. 2(iii) also shows similarity of the atomic arrangements of the liquid Al adjacent to the three substrates at the simulation time t = 500 fs.

Next we have a closer look at the atomic occupation of the terminating sites at the substrates. The snapshots of the terminating Al layers for the interfaces at the simulated time, t = 0.5 ps are displayed in Fig. 2(iv). These terminating atoms display split along the direction perpendicular to the substrate, forming uneven layers which contain vacancies. The Al occupation ratios of the terminating sites are 51.9%, 59.3%, 66.7% for the L-Al/α-Al_2O_3{0 0 0 1}$_O$, L-Al/α-Al_2O_3{0 0 0 1}$_{1Al}$ and L-Al/α-Al_2O_3{0 0 0 1}$_{2Al}$ systems, respectively. The first two values are lower than that with the O-fixed system (66.7%). The simulations also showed variation of Al occupation of the sites at the termination layer on longer simulation time. For example, the Al occupation of the sites at the terminating layer in the L-Al/α-Al_2O_3{0 0 0 1}$_{2Al}$ decreases with time and converges to about 56%. This will be discussed in a following section.

Fig. 3 shows the behavior of the total-valence-electron (free) energy of the L-Al/α-Al_2O_3{0 0 0 1}$_{2Al}$ system during the *AI*MD simulation. The energy decreases quickly with time at beginning and reaches the equilibration value in about 1.5 ps. This indicates that the formation of an Al terminating layer to the substrates proceeds in a couple of picoseconds. This agrees with the observations that there are no significant differences for the systems with different starting configurations (Table 1) after about 1.5 ps. Therefore, we will not distinguish them in the rest of the manuscript.

In brief, after a period of evolutions (~1.5 ps) the resultant liquid Al/oxide interfaces from the different starting configurations become equilibrated and resulted in similar configurations. In the L-Al/α-Al_2O_3{0 0 0 1} systems forms an Al layer terminating the substrate and therefore, and the system is renamed as L-Al/α-Al_2O_3{0 0 0 1}$_{Al}$. Similarly, we denote the equilibrated liquid-Al/MgO{1 1 1} system which terminates with an Al layer, as L-Al/MgO{1 1 1}$_{Al}$.

3.2. Prenucleation at the liquid/oxide interfaces

Fig. 4 shows snapshots of the equilibrated L-Al/MgO{1 1 1}$_{Al}$ (a), the L-Al/α-Al_2O_3{0 0 0 1}$_{Al}$ (b) and the L-Al/α-Al_2O_3{0 0 0 1}$_{Al}$ system with the O-atoms fixed (c) as a reference. Clearly, there is an Al layer

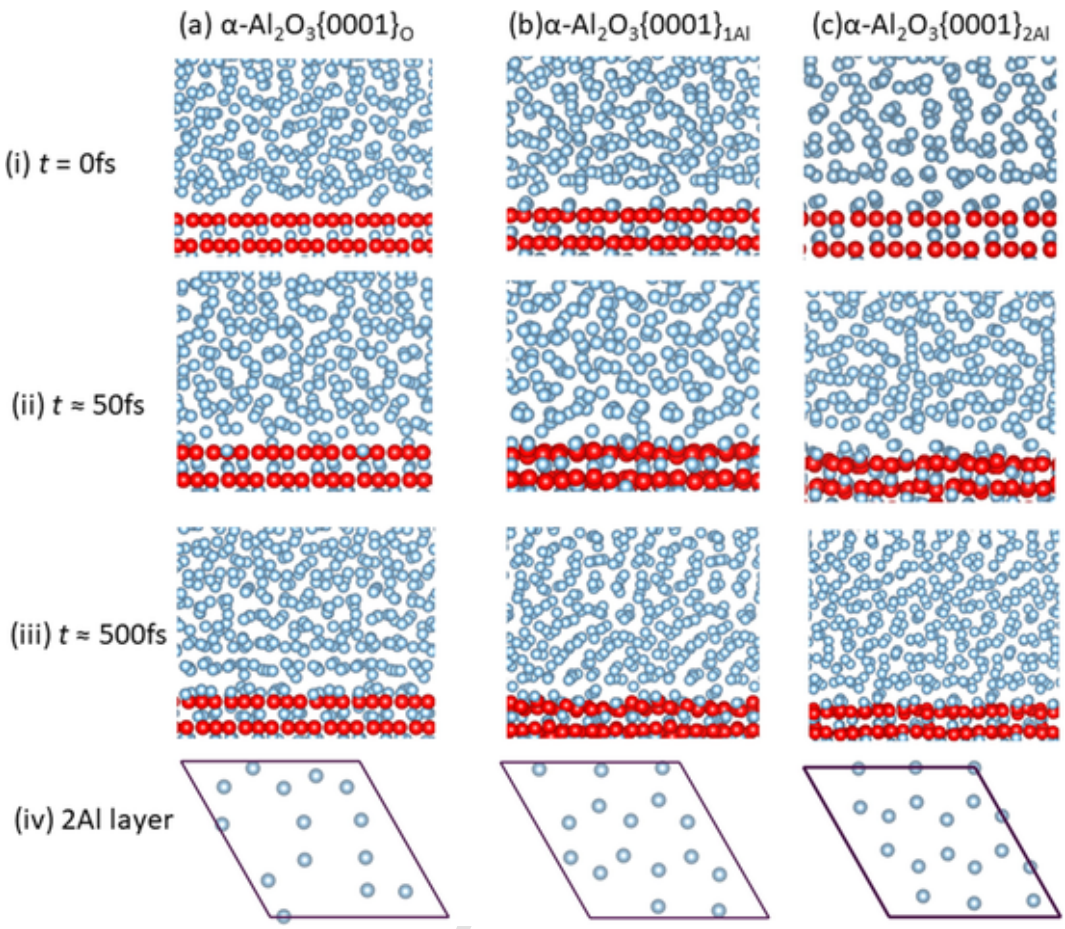

Fig. 2. Snapshots of the structural evolutions of the L-Al/α-Al_2O_3{0 0 0 1} interfaces with different starting configurations during *AI*MD dynamics simulations at 1000 K. Fig. 2(iv) shows snapshots of the corresponding atomic structures of the terminating Al layers of the simulated systems at 0.5 ps. Note that the terminating Al-layers are split and uneven as shown in 2iii. The silvery spheres represent Al and red for O. The violet lines in Fig. 2iv represent the in-plane axis of the unit cells. (For interpretation of the references to color in this figure legend, the reader is referred to the web version of this article.)

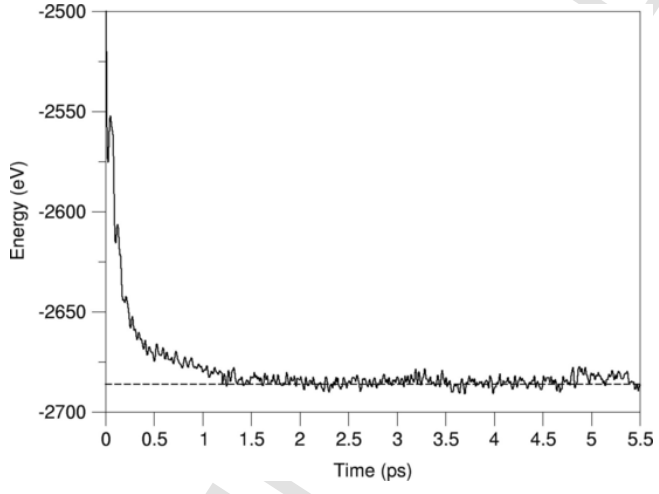

Fig. 3. Variation of the total valence-electron energy of the L-Al/α-Al_2O_3{0 0 0 1}$_{2Al}$ system during *AI*MD dynamics simulations at 1000 K. The dashed line represents the equilibrated energy of the system at 1000 K.

terminating both the α-Al_2O_3{0 0 0 1} and the MgO{1 1 1} substrates in all cases. Fig. 5 displays the atomic density profiles of the liquid Al atoms adjacent to the interfaces for the systems. The density profiles were obtained via Eq. (1) with the configurations simulated for 4.5 ps.

The frame of the density profile of the L-Al/MgO{1 1 1}$_{Al}$ system (Fig. 5a) is similar to that of the Al_2O_3{0 0 0 1}$_{Al}$ system (Fig. 5b). In both cases the terminating Al-layer exhibits complex structure: The Al-layer terminating the MgO{1 1 1} substrate consists of a sharp peak and a shoulder. The space between the peak and the shoulder is about 0.8 Å away (Fig. 5a). The terminating Al-layer in the L-Al/α-Al_2O_3{0 0 0 1}$_{Al}$ system exhibits two clear sub-peaks with peak gap of 0.6 Å (Fig. 5b). The splitting of the terminating Al-layer is stronger in the O-fixed system (Fig. 5c).

Such splitting of the Al-terminating layer is similar to that in the bulk α-Al_2O_3 (Fig. 1a). The splitting of the terminating Al layer is demonstrated by the examples of the interfacial chemical bonding for the L-Al/MgO{1 1 1}$_{Al}$ (Fig. 6a) and L-Al/α-Al_2O_3{0 0 0 1}$_{Al}$ (Fig. 6b) systems, respectively. There are more Al atoms closer to the O at the L-Al/MgO{1 1 1}$_{Al}$ interface (Fig. 6a), corresponding to the rather sharp peak as compared with the smaller shoulder (Fig. 5a). Meanwhile, the Al atoms terminating the α-Al_2O_3{0 0 0 1} substrate display a broader range, corresponding to the broad peaks of the Al1 and Al2 sublayers as (Fig. 5b).

Here we analyse the Al occupation of the terminating sites on the substrates. Statistics analysis for the configurations over 3.0 ps provided that the Al occupation ratio of the terminating sites at the L-Al/MgO{1 1 1}$_{Al}$ interface is 73.3%, meanwhile the Al occupation ratio at the L-Al/α-Al_2O_3{0 0 0 1}$_{Al}$ interface is 55.9%. The latter number is in line with those in Fig. 2(iv). This value agrees with the recent work [27]. The Al occupation of the terminating sites at the L-Al/α-

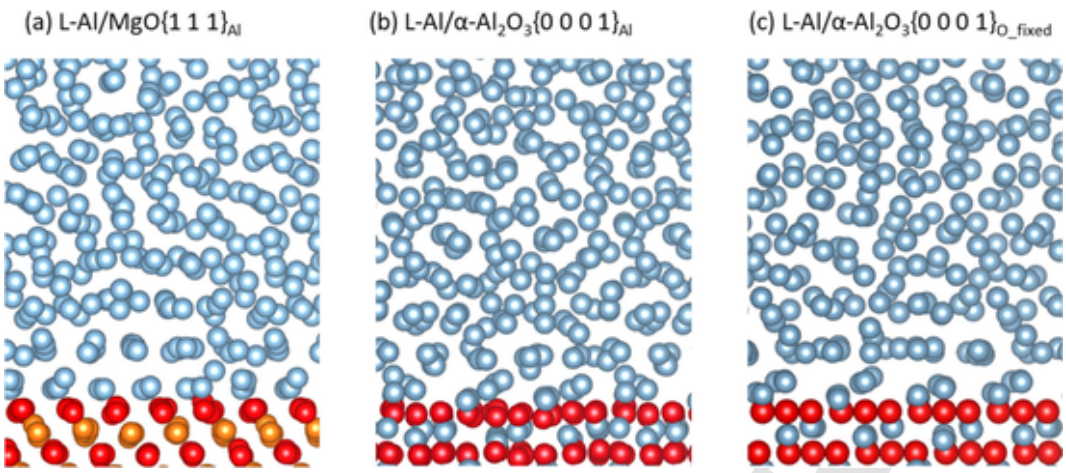

Fig. 4. Snapshots of the structures of the equilibrated L-Al/MgO{1 1 1}$_{Al}$ (a) and L-Al/α-Al_2O_3{0 0 0 1}$_{Al}$ systems. Fig. 4c shows the snapshot of the L-Al/α-Al_2O_3{0 0 0 1}$_{Al}$ system with the O-atoms pinned. The silvery spheres represent Al, the golden Mg and the red O. (For interpretation of the references to color in this figure legend, the reader is referred to the web version of this article.)

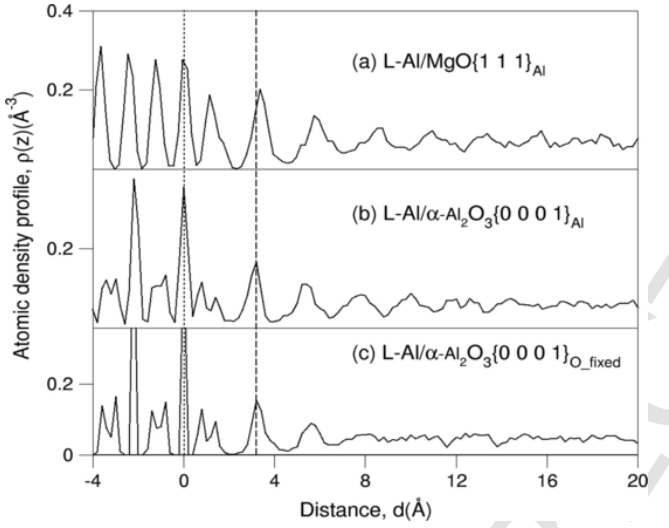

Fig. 5. Atomic density profiles of the equilibrated systems. The dotted line at 0.0 Å indicates the peak of the outmost O layer, the dashed line the 1st Al layer in the L-Al/α-Al_2O_3{0 0 0 1}$_{Al}$ systems.

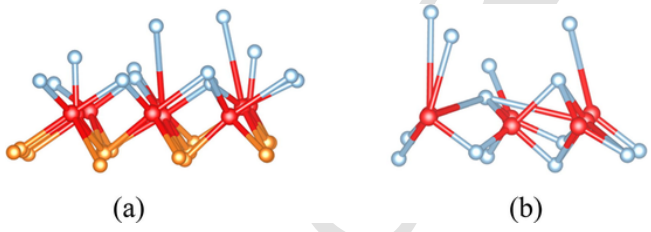

Fig. 6. Local chemical bonding at the equilibrated L-Al/MgO{1 1 1}$_{Al}$ (a) and L-Al/α-Al_2O_3{0 0 0 1}$_{Al}$ (b) interfaces. The silvery spheres represent Al, the golden Mg and the red O. (For interpretation of the references to color in this figure legend, the reader is referred to the web version of this article.)

Al_2O_3{0 0 0 1}$_{Al}$ interface with the O-layers fixed is 66.7% (Fig. 2(iv)), high than the relaxed system. This indicates importance of full-relaxation in study of liquid/solid interfaces.

Figs. 4 and 5 provide details about the layering in the liquid adjacent to the L-Al/oxide interfaces. The terminating Al-layer is well separated from the nearby liquid atoms on MgO{1 1 1}$_{Al}$, whereas they are admixed with each other on the α-Al_2O_3{0 0 0 1}$_{Al}$ substrate. There are three/four distinct peaks in the liquid adjacent to the L-Al/MgO{1 1 1}$_{Al}$ and the L-Al/α-Al_2O_3{0 0 0 1}$_{Al}$ interface. The latter is similar to the recent simulations [27]. Moreover, the analysis also produced that the distance between the first Al peak and the outmost O layer in the L-Al/MgO{1 1 1}$_{Al}$ system is slightly larger than that in the L-Al/α-Al_2O_3{0 0 0 1}$_{Al}$ system (Fig. 5). This is unexpected since the latter has a slightly shorter in-plane *a*- and *b*-axis (Table 1).

The epitaxial nucleation model indicates that the atomic arrangement of the substrate surface templates the formation of the solid at the interface [4,49]. We presented the snapshots of the important atomic layers at the interfaces in Fig. 7. To quantify the atomic ordering, we also analysed the in-plane ordering parameters for the individual atomic layers using the summed configurations of simulations for 3.0–4.5 ps via equation (2). The results were plotted in Fig. 8.

The snapshots displayed that the outmost O-layers of both interfaces are well-ordered (Fig. 7). There are atomic vacancies and displacements at both terminating Al layers. The Al atoms terminating the MgO{1 1 1} have a higher occupation than those terminating the α-Al_2O_3{0 0 0 1}, in agreement with our previous analysis. The 1st Al-layers exhibit vacancies and disordering.

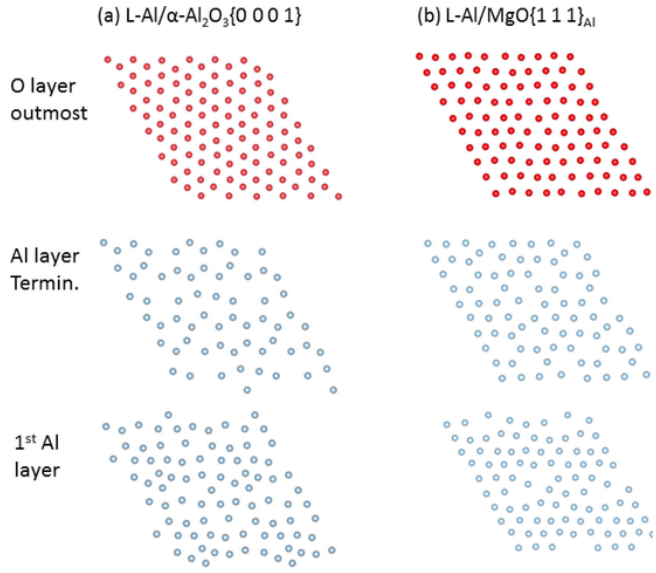

Fig. 7. Snapshots of the atomic configurations for important atomic layers in the L-Al/α-Al_2O_3{0 0 0 1} (a) and L-Al/MgO{1 1 1}$_{Al}$ (b) systems. The silvery spheres represent Al and the red O. (For interpretation of the references to color in this figure legend, the reader is referred to the web version of this article.)

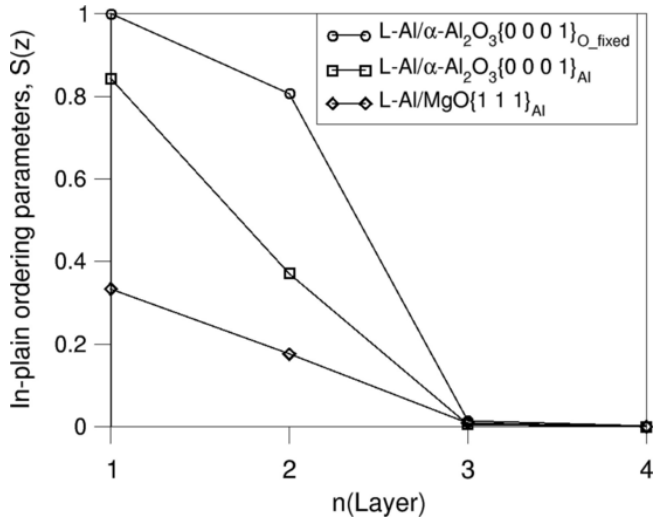

Fig. 8. In-plane ordering parameters of the equilibrated L-Al/α-Al_2O_3{0 0 0 1} and L-Al/MgO{1 1 1}$_{Al}$ systems at 1000 K. At the *x*-axis, $n = 1$ represent the outmost O-layers, $n = 2$ the terminating Al-layers, 3 the 1st Al layer and 4 the 2nd Al layers.

Fig. 8 shows the in-plane ordering parameters for the two systems. In the Al/MgO{1 1 1}$_{Al}$ system, the in-plane ordering parameter for the O-layers in the substrate decreases quickly from bulk to the interface from 0.65 (bulk) to 0.52 (second to the surface) and 0.33 (the outmost O-layer, Fig. 8). The in-plane ordering parameter of the outmost O layer at the L-Al/Al_2O_3{0 0 0 1}$_{Al}$ interface is 0.82 which is close to that in bulk 0.85). This corresponds to electronic band theory analysis that for these ionic crystals, the oxygen lattices determine the structures of these ionic oxides according to the electronic structure theory [19,20]. The larger n(O)/n(Al) ratio in Al_2O_3 (2/3) than that of MgO (1/1) means higher stability of α-Al_2O_3{0 0 0 1} than MgO{1 1 1} in Al liquid.

Fig. 8 shows that the in-plane ordering decreases quickly in the liquid Al layers. The $S(z)$ values lower to about halves of those of the outmost O-layer for both fully-relaxed systems (Fig. 8). Meanwhile the small decrease of the $S(z)$ value for the terminating Al layer in the L-Al/α-Al_2O_3{0 0 0 1} system with the substrate O fixed. This indicates the importance of relaxation of substrate atoms to describe the interfaces in a reliable way. The in-plane ordering of the 1st Al layers in all simulated systems diminishes to nearly zero in all the simulated systems.

We also performed *ab initio* molecular dynamics simulations for liquid Al on the Mg-terminated MgO{1 1 1} substrate (L-Al/MgO{1 1 1}$_{Mg}$). The simulations provided a uniquely Mg termination layer. The Mg atoms at this layer are well-ordered. Meanwhile, they are partially charged. The simulations revealed that the prenucleation in the liquid Al adjacent to the L-Al/MgO{1 1 1}$_{Mg}$ interface is higher than those at the atomically rough MgO{1 1 1}$_{Al}$ and the α-Al_2O_3{0 0 0 1} substrates. The details of the results are out of the present scope and will be presented elsewhere.

In conclusion, at the L-Al/Al_2O_3{0 0 0 1}$_{Al}$ and the L-Al/MgO{1 1 1}$_{Al}$ interfaces there is an atomically rough Al layer terminating the substrates. The rough Al-layers have weak templating power and therefore, cause weak prenucleation at the liquid-Al/oxide interfaces.

3.3. Chemical bonding and interaction at the liquid/oxide interfaces

In order to get insight into the prenucleation at the L-Al/oxide interfaces, we analysed the electronic properties at the interfaces. Fig. 9 displays the *iso*-surfaces of the electronic density distributions at the two equilibrated systems. There are randomly distributed clouds in the liquid parts, in agreement with the free-electron picture for liquid Al. In the substrates appear regular large O spheres together with small Al and Mg spheres. This picture evidences the ionic nature of the oxide substrates. At the interfaces, there are electron clouds and Al ions in touch with the O spheres, indicating interfacial interaction.

Charges at and charge transfer between atoms provide a direct understanding of the interfacial interaction. Fig. 10 shows the charges at the atomic sites at the two studied interfaces using the Bader charge approach [50,51]. This method was implanted into the code VASP [52].

The Bader charges in the substrates are −1.3e/O, +1.3/Mg and +2.0/Al, which agree with the ionic model (O^{-2}, Mg^{+2} and Al^{+3}) at first approximation. The smaller values indicate certain content of covalence [53]. The liquid Al atoms in the liquid away from the substrate surfaces are around zero, being electronically neutral.

The Bader analysis reveals that the terminating Al atoms/ions are positively charged with the value decreasing with increasing distance. Interestingly, the Al atoms at the first Al-layer at the L-Al/Al_2O_3{0 0 0 1}$_{Al}$ lose a little electrons. This indicates interfacial interaction in this system. Meanwhile, the liquid Al atoms in the 1st Al-layer in the L-Al/MgO{1 1 1}$_{Al}$ are neutral (Fig. 10). This explains the

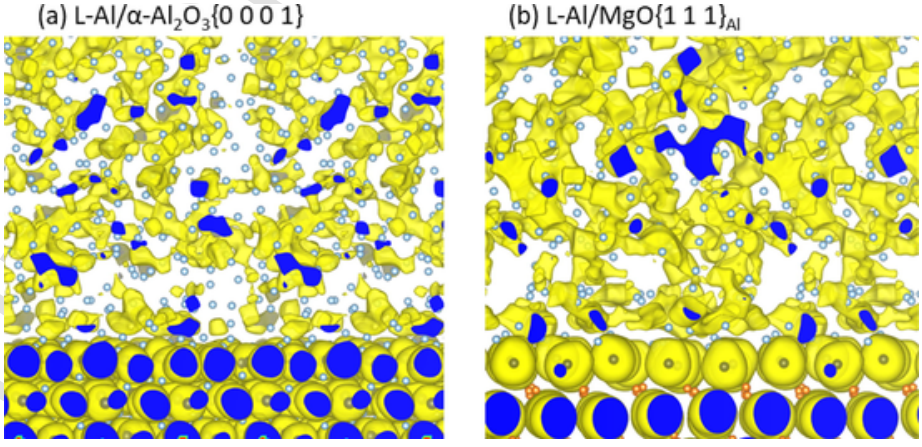

Fig. 9. Iso-surfaces of electron density at the L-Al/α-Al_2O_3{0 0 0 1}$_{Al}$ and L-Al/MgO{1 1 1}$_{Al}$ interfaces. The yellow spheres represent the *iso*-surfaces with electron density $\rho(\mathbf{r}_0) = 0.037$e/Å^3. The blue regions have higher electron densities whereas the white regions have lower values. The small golden spheres represent Mg and silvery Al nuclei. The O ions (dark blue spheres) are hidden in the electron spheres. (For interpretation of the references to color in this figure legend, the reader is referred to the web version of this article.)

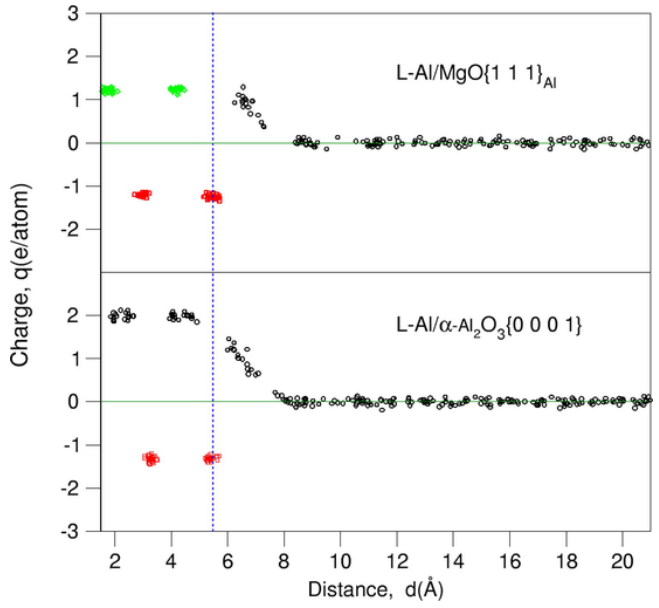

Fig. 10. The charge profiles for the L-Al/α-Al_2O_3{0 0 0 1}$_{Al}$ and L-Al/MgO{1 1 1}$_{Al}$ systems. The red squares represent charges at O, the black spheres at Al, the orange diamonds Mg. (For interpretation of the references to color in this figure legend, the reader is referred to the web version of this article.)

smaller spacing between the substrate to the 1st Al layer in the L-Al/Al_2O_3{0 0 0 1}$_{Al}$ system than that in the L-Al/MgO{1 1 1}$_{Al}$ system.

4. Discussion

As mentioned before, both MgO and Al_2O_3 are ionic compounds. The outmost O-layer of both MgO{1 1 1} and α-Al_2O_3{0 0 0 1} substrates is composed of a close-packed hexagonal lattice which O atoms are partially charged (−1e) in the ionic model. Therefore, the substrates require the same amount of electrons from the liquid Al to reach charge balance. One would expect same occupation of the terminating sites by Al for at substrates.

The *AI*MD simulations provide different occupation ratios of the terminating sites: L-Al/MgO{1 1 1}$_{Al}$ (73.3%), L-Al/Al_2O_3{0 0 0 1}$_{Al}$ (55.9%). The smaller Al occupation ratio of the terminating sites in L-Al/Al_2O_3{0 0 0 1}$_{Al}$ (55.9%) is compensated by the extra charge transfer from the 1st Al layer. Consequently, the atomic spacing between the 1st Al-layer to the outmost O-layer in the L-Al/Al_2O_3{0 0 0 1}$_{Al}$ system is shorter than that in the L-Al/MgO(1 1 1}$_{Al}$ system, though the latter has a smaller in-plane surface (Table 1).

The present *AI*MD simulations provided that there is a terminating Al layer on α-Al_2O_3{0 0 0 1}$_{Al}$ or MgO{1 1 1}$_{Al}$ in liquid Al. This Al layer is split and contains vacancies, being atomically rough. These Al atoms at the layers terminating both substrates are partially charged. The atomically rough and partially ionized Al layers hinder the prenucleation of nearby liquid Al. There are only two or three distinct Al-layers in the liquid adjacent to the interfaces. The layering is notably weaker as compared with those on a smooth metallic substrate (typically 6 layers [5–7,37]). There is also little in-plane ordering of the 1st Al-layer in both systems. Therefore, the atomic roughness of the terminating Al-layers hinders atomic ordering in the liquid adjacent to a liquid/substrate interface, in line with the recent work [38].

As mentioned before, prenucleation refers to the atomic ordering in the liquid adjacent to the liquid/substrate interface at temperatures above the nucleation temperature [6,7,49]. Therefore, the potency of a substrate for heterogeneous nucleation can be related to the degree of prenucleation [6,7,49]. Previous *ab initio* molecular dynamics simulations produced pronounced prenucleation in liquid Al adjacent to the Ti-terminated TiB_2 substrate (TiB_2{0 0 0 1}$_{Ti}$) [54–56]. This agrees with experimental observations that TiB_2 particles with excess Ti are excellent grain refiners for solid Al [2,57]. Based on the results of the atomic ordering in the liquid at the interfaces, we can conclude that the nucleation potency of both MgO{1 1 1}$_{Al}$ and Al_2O_3{0 0 0 1}$_{Al}$ substrates to α-Al is weak.

In heterogeneous nucleation processes, a more potent substrate requires a smaller driving force (undercooling) to nucleate the metal. Therefore, for the less potent α-Al_2O_3{0 0 0 1}$_{Al}$ and MgO{1 1 1}$_{Al}$ substrates, the nucleation requires larger undercooling and the nucleation temperatures can even be lower than the grain-initiation temperature. As soon as the nucleation temperature is reached, nucleation occurs and grain initiation follows immediately. In such cases, nucleants of smaller sizes have the opportunity to function and the number of efficient nucleation sites should be much larger than the traditional grain-refiners which only the large particles can survive [1–3,49]. The nucleation and grain initiation processes occur almost simultaneously in an explosive way [49]. Such as explosive grain initiation produces fine grains of the solidified alloys if a large number of substrate particles were distributed homogeneously.

5. Conclusions

We investigated the prenucleation at the L-Al/α-Al_2O_3{0 0 0 1}$_{Al}$ and the L-Al/MgO{1 1 1}$_{Al}$ interfaces. Based on the simulations, the following conclusions can be attained:

1) At thermal equilibrium, an Al-layer forms and terminates the MgO{1 1 1} and α-Al_2O_3{0 0 0 1} substrates in liquid Al. These newly formed terminating Al-layers are split and contain atomic vacancies and displacements, being atomically rough.
2) There is still certain context of charge transfer occurring from the Al atoms in the 1st Al layer to the outmost O-layer in the L-Al/α-Al_2O_3{0 0 0 1} system. This causes smaller spacing between the substrate surface and the 1st Al layer in the system.
3) There is weak prenucleation at the L-Al/α-Al_2O_3{0 0 0 1}$_{Al}$ and the L-Al/MgO{1 1 1}$_{Al}$ interfaces. This indicates nucleation weak potency of these substrates to α-Al.

Declaration of Competing Interest

The authors declare that they have no known competing financial interests or personal relationships that could have appeared to influence the work reported in this paper.

Acknowledgement

His work was supported by Engineering and Physical Sciences Research Council (EPSRC, UK) under grant number EP/N007638/1.

References

[1] K.F. Kelton, A.L. Greer, Nucleation in condensed matter: applications in materials and biology, Pergamon Materials Series, Elsevier Ltd., Oxford/Amsterdam, 2010.
[2] A.L. Greer, Overview: application of heterogeneous nucleation in regain-refining of metals, J. Chem. Phys. 145 (2016), doi:10.1063/1.4968846 211704.
[3] M.A. Easton, M. Qian, A. Prasad, D.H. StJohn, Recent advances in grain refinement of light metals and alloys, Curr. Opin. Solid State Mater. Sci. 20 (2016) 13–24, doi:10.1016/j.cossms.2015.10.001.
[4] Z. Fan, An epitaxial model for heterogeneous nucleation on potent substrate, Metall. Mater. Trans. A 44 (2013) 1409–1418, doi:10.1007/s11661-012-1495-8.
[5] H. Men, Z. Fan, Atomic ordering in liquid aluminium induced by substrates with misfits, Comput. Mater. Sci. 85 (2014) 1–7, doi:10.1016/j.commatsci.2013.12.042.
[6] H. Men, Z. Fan, Prenucleation induced by crystalline substrates, Metall. Mater. Trans. A 49 (2018) 2766–2777, doi:10.1007/s11661-018-4628-x.
[7] C.M. Fang, H. Men, Z. Fan, Effect of substrate chemistry on prenucleation, Metall. Mater. Trans. A 49 (2018) 6231–6242, doi:10.1007/s11661-018-4882-y.
[8] Y. Wang, H.-T. Li, Z. Fan, Oxidation of aluminium alloy melts and inoculation by oxide particles, Trans. Indian Inst. Met. 65 (2012) 653–661, doi:10.1007/s12666-012-0194-x.

[9] Y. Wang, H.-T. Li, Z. Fan, G. Scamans, Characterization of oxide films in Al-Mg alloy melts, Mater. Sci. Forum 765 (2013) 220–224, doi:10.4028/www.scientific.net/MSF.765.220.
[10] Z. Fan, Y. Wang, M. Xia, S. Arumuganathar, Enhanced heterogeneous nucleation I AZ91D alloy by intensive met shearing, Acta Mater. 57 (2009) 4891–4901, doi:10.1016/j.actamat.2009.06.052.
[11] Y. Wang, Z. Fan, X. Zhou, G.E. Thompson, Characterisation of magnesium oxide and its interface with α-Mg in Mg-Al-based alloys, Philos. Mag. Lett. 91 (2011) 516–529, doi:10.1080/09500839.2011.591744.
[12] H. Men, B. Jiang, Z. Fan, Mechanisms of grain refinement by intensive shearing AZ91 alloy melt, Acta Mater. 58 (2010) 6526–6534, doi:10.1016/j.actamat.2010.08.016.
[13] K. Kim, Formation of endogenous MgO and $MgAl_2O_4$ particles and their possibility of acting as substrate for heterogeneous nucleation of aluminium grains, Surf. Interface Anal. 47 (2015) 429–439, doi:10.1002/sia.5726.
[14] K. Kim, FIB serial milling and lifting out of fine inclusions in an intensively melt sheared aluminium alloy, Mater. Lett. 117 (2014) 74–77, doi:10.1016/j.matlet.2013.11.083.
[15] L. Wang, L. Yang, D. Zhang, M. Xia, Y. Wang, J.G. Li, The role of lattice misfit on heterogeneous nucleation of pure aluminium, Metall. Mater. Trans. A 47 (2016) 5012–5022, doi:10.1007/s11661-016-3691-4.
[16] Z.P. Que, Y.P. Zhou, Z. Fan, Effect of MgO on phase selections in Al-Mg-Si-Fe-Mn alloys, Trans. Indian Inst. Met. 68 (2015) 1167–1172, doi:10.1007/s12666-015-0664-z.
[17] G. Fiquet, P. Richet, G. Montagnac, High-temperature thermal expansion of lime, periclase, corundum and spinel, Phys. Chem. Miner. 27 (1999) 103–111, doi:10.1007/s002690050246.
[18] R.R. Reeber, K. Goessel, K. Wang, Thermal expansion and molar volume of MgO, periclase, from 5 to 2900K, Eur. J. Mineral. 7 (1995) 1039–1048, doi:10.1127/ejm/7/5/1039.
[19] P.K. de Boer, R.A. de Groot, The conduction bands of MgO, MgS and HfO_2, J. Phys.: Condens. Matter 10 (1998) 10241–11248, doi:10.1088/0953-8984/10/45/011.
[20] C.M. Fang, R.A. de Groot, The nature of electron states in AlN and α-Al_2O_3, J. Phys.: Condens. Matter 19 (2007), doi:10.1088/0953-8984/19/38/386223.
[21] P.W. Tasker, The surface energies, surface tensions and surface structure of the alkali halide crystals, Philos. Mag. A 39 (1979) 119–136, doi:10.1080/01418617908236887.
[22] C. Noguera, Polar oxide surfaces, J. Phys.: Condensed Matter 12 (2000) R367–R410, doi:10.1088/0953-8984/12/31/201.
[23] C.M. Fang, Z. Fan, Prenucleation at the interface between MgO and liquid magnesium: An ab initio molecular dynamics study, to be submitted.
[24] S.H. Oh, Y. Kauffmann, C. Scheu, W.D. Kaplan, Rühle, Ordered liquid aluminium at the sapphire, Science 310 (2005) 661–663, doi:10.1126/science.1118611.
[25] Y. Kauffmann, S.H. Oh, C.T. Koch, A. Hashibon, C. Scheu, M. Rühle, W.D. Kaplan, Quantitative analysis of layering and in-plane ordering structural ordering at an alumina-aluminium solid liquid interface, Acta Mater. 59 (2011) 4378–4386, doi:10.1016/j.actamat.2011.03.061.
[26] M. Gandman, Y. Kauffmann, C.T. Koch, W.D. Kaplan, Direct quantification of ordering at a solid-liquid interface using aberration corrected transmission electron microscopy, Phys. Rev. Lett. 110 (2013), doi:10.1103/PhysRevLett.110.086106 086106.
[27] S.D. Ma, A.J. Brown, R. Yan, R.L. Davidchack, P.B. Howes, C. Nicklin, Q.J. Zhai, T. Jing, H.B. Dong, Atomistics of prenucleation layering of liquid metals at the interface with poor nucleants, Commun. Chem. 2 (2019) 1, doi:10.1038/s42004-018-0104-1.
[28] T. Hong, J.R. Smith, D.J. Srolovitz, Metal/ceramic adhesion: a first-principles study of MgO/Al and MgO/Ag, J. Adhesion Sci. Technol. 8 (2012) 837–851, doi:10.1163/156856194X00474.
[29] A.J. Mcevoy, R.H. Williams, I.G. Higginbotham, Metal/non-metal interfaces. The wetting of magnesium oxide by aluminium and other metals, J. Mater. Sci. 11 (1976) 297–302, doi:10.1007/BF00551441.
[30] P. Shen, H. Fuji, T. Matsumoto, K. Nogi, Wetting and reaction of MgO single crystals by molten Al, Acta Mater. 52 (2004) 887–898, doi:10.1016/j.actamat.2003.10.024.
[31] T. Wagner, M. Rühle, Growth and structure of Al/MgO interfaces, MRS Online Proc. 357 (1994) 41, doi:10.1557/PROC-357-41.
[32] G. Levi, W.D. Kaplan, Aluminium-alumina interface morphology and thermodynamics from dewetting experiments, Acta Mater. 51 (2003) 2793–2802, doi:10.1016/S1359-6454(03)00084-3.
[33] G. Dehm, B.J. Inkson, T. Wagner, Growth and microstructural stability of epitaxial Al films on (0001)α-Al_2O_3 substrates, Acta Mater. 50 (2002) 5021–5032, doi:10.1016/S1359-6454(02)00347-6.
[34] D.L. Medlin, K.F. McCarty, R.Q. Hwang, S.E. Guthrie, M.I. Basks, Orientation relations in heteroepitaxial aluminium films on sapphire, Thin Solid Films 299 (1997) 110–114, doi:10.1016/S0040-6090(96)09393-5.
[35] J. Kang, J. Zhu, C. Curtis, D. Blake, G. Glazmaier, Y.-H. Kim, S.-H. Wei, Atomically abrupt liquid oxide interface stabilized by self-regulated interfacial defects: the case of Al/Al_2O_3 interfaces, Phys. Rev. Lett. 108 (2012), doi:10.1103/PhysRevLett.108.226105 226105.
[36] A. McLeod, C. Gabryel, Kinetics of the growth of spinel, $MgAl_2O_4$, on alumina particulate in aluminium alloys containing magnesium, Metall. Mater. Trans. A 23 (1992) 1279–1283, doi:10.1007/BF02665059.
[37] A. Hashibon, J. Adler, M.W. Finnis, W.D. Kaplan, Atomistic study of structural correlations at a liquid-solid interface, Comput. Mater. Sci. 24 (2002) 443–452, doi:10.1016/S0927-0256(01)00265-8.
[38] B. Jiang, H. Men, Z. Fan, Atomic ordering in the liquid adjacent to an atomically rough solid surface, Comput. Mater. Sci. 153 (2018) 73–81, doi:10.1016/j.commatsci.2018.06.005.
[39] J.W. Arblaster, Selected Values of the Crystallographic Properties of the Elements, ASM International Materials Park, Ohio, 2018.
[40] L.E. Hintzsche, C.M. Fang, M. Marsman, G. Jordan, M.W.P.E. Lamers, A.W. Weeber, G. Kresse, Density functional theory study of the structural and electronic properties of amorphous silicon nitrides: Si_3N_{4-x}:H, Phys. Rev. B 86 (2012), doi:10.1103/PhysRevB.86.235204 235204.
[41] C.M. Fang, W.F. Li, R.S. Koster, J. Klimes, A. van Blaaderen, M.A. van Huis, The accurate calculation of the band gap of liquid water by means of GW corrections applied to plane-wave density functional theory molecular dynamics simulations, PCCP 17 (2015) 365–375, doi:10.1039/C4CP04202F.
[42] G. Kresse, J. Hafner, Ab initio molecular-dynamics simulation of the liquid-metal-amorphous-semiconductor transition in germanium, Phys. Rev. B 49 (1994) 14251–14269, doi:10.1103/PhysRevB.49.14251.
[43] G. Kresse, J. Furthmüller, Efficiency of ab-initio total energy calculations for metals and semiconductors using a plane-wave basis set, Comp. Mater. Sci. 6 (1996) 15–50, doi:10.1016/0927-0256(96)00008-0.
[44] P.E. Blöchl, Projector augmented-wave method, Phys. Rev. B 50 (1994) 17953–17978, doi:10.1103/PhysRevB.50.17953.
[45] G. Kresse, J. Joubert, From ultrasoft pseudopotentials to the projector augmented-wave method, Phys. Rev. B 59 (1999) 1758–1775, doi:10.1103/PhysRevB.59.1758.
[46] J.P. Perdew, K. Burke, M. Ernzerhof, Generalized gradient approximation made simple, Phys. Rev. Lett. 77 (1996) 3865–3868, doi:10.1103/PhysRevLett.77.3865.
[47] H.J. Monkhorst, J.D. Pack, Special points for Brillouin-zone integrations, Phys. Rev. B 13 (1976) 5188–5192, doi:10.1103/PhysRevB.13.5188.
[48] L.E. Hintzsche, C.M. Fang, M. Marsman, G. Jordan, M.W.P.E. Lamers, A.W. Weeber, G. Kresse, Defects and defect healing in amorphous $Si_3N_{4-x}H_y$: an ab initio density functional theory study, Phys. Rev. B 88 (2013), doi:10.1103/PhysRevB.88.155204 155204.
[49] Z. Fan, Heterogeneous nucleation, grain initiation and grain refinement of Mg alloys, in: Z. Fan, C. Mendis (Eds.), Proceedings of the 11th International Conference on Magnesium Alloys and Their Applications, Beaumount Estate, Old Windsor, UK, 2018, p. 17.
[50] R.F.W. Bader, Atoms in Molecules: A Quantum Theory, Oxford University Press, New York, 1990.
[51] R.F.W. Bader, A bond path: a universe indicator of bonded interactions, J. Phys. Chem. A 102 (1998) 7314–7323, doi:10.1021/jp981794v.

[52] G. Henkelman, A. Arnaldsson, H. Jónsson, A fast and robust algorithm for Bader decomposition of charge density, Comput. Mater. Sci. 36 (2006) 354–360, doi:10.1016/j.commatsci.2005.04.010.
[53] I.D. Brown, The Chemical Bond in Inorganic Chemistry: The Bond Valence Model, Oxford University Press, 2002.
[54] J.S. Wang, A. Horsfield, U. Schwingenschlogl, P.D. Lee, Heterogeneous nucleation of solid Al from the melt by TiB_2 and Al_3Ti: an ab initio molecular dynamics study, Phys. Rev. B 82 (2010), doi:10.1103/PhysRevB.82.184203 184203.
[55] J.S. Wang, A.P. Horsfield, P.D. Lee, P. Brommer, Heterogeneous nucleation of sloid A from the melt Al3Ti: molecular dynamics simulations, Phys. Rev. B 82 (2010), doi:10.1103/PhysRevB.82.144203 144203.
[56] D. Wearing, A.P. Horsfield, W.W. Xu, P.D. Lee, Which wets TiB2 inoculant particles: AL or Al3Ti?, J. Alloys Compd. 664 (2016) 460–468, doi:10.1016/j.jallcom.2015.12.203.
[57] A. Cibula, The mechanisms of grain refinement in dilute aluminium-alloys, Metal. Trans. 3 (1972) 751, doi:10.1007/BF02642770.